



## Influence of Engineering Properties on Radiation Shielding Characteristics of Some Egyptian Granitic Rocks as Potential Materials



H.A. Farag<sup>1</sup>, W.M. Draz<sup>1</sup>, Faisal A. Ali<sup>1\*</sup>, M.M. Arfa<sup>2</sup>, R.M. El Shazly<sup>2</sup>, M.M. Sadawy<sup>1</sup>, A.T.M. Farag<sup>2</sup>

<sup>1</sup> Al-Azhar University, Faculty of Engineering, Mining and Pet. Dept., Nasr City, 11371, Cairo, Egypt.

<sup>2</sup> Physics Department, Faculty of Science, Al-Azhar University, Nasr City, 11884, Cairo, Egypt

### Abstract

In the present study, chemical, mineralogical compositions, petrographic characteristics, physical and mechanical properties and the radiation shielding characteristics of some Egyptian granitic rocks were established and compared with two types of concrete as reference materials (ordinary concrete (OC) and reactive powder concrete (RPC)). Two neutron types, namely slow neutron and neutron with energy greater than 10 keV have been employed for calculating the macroscopic neutron cross-sections ( $\Sigma$ , cm<sup>-1</sup>). Different gamma ray energy lines ranged from 121.78 to 1407.92 keV were utilized for evaluating mass attenuation coefficients of gamma rays. Gamma shielding parameters were tested and computed. The results indicated that in the case of fast neutrons, the  $\Sigma_{10}$  for rocks is greater than that of OC and RPC of about 45%, while in the case of slow neutrons,  $\Sigma S$  is greater than that of OC and RPC of about 18%. Further, the results indicated that the three rock types have attenuation behavior favorable than that of OC and RPC in all used  $\gamma$ -rays energies. On the other hand, the calculated mass attenuation coefficient (MAC) using WinXcom computer program and the experimental values showed excellent agreements.

**Keywords:** Radiation shielding materials, Attenuation parameters, mineralogical compositions and engineering properties.

**Keywords:** Radiation shielding materials; Attenuation parameters; mineralogical compositions and engineering properties

### 1. Introduction

Owing to the limitation of fossil fuel resources, nuclear power is an alternative source for many countries [1-3]. Additionally, thermal neutron treatment for boron-neutron capture and fast neutron external beam radiation are both crucial applications for slow and fast neutrons in medicine [4]. New sources of radionuclides for usage in diverse applications are mostly created using slow neutrons [5]. Neutron exposure, however, carries a significant danger and might have negative impacts on both the public and the workers [6]. The health risks brought on by radiation exposure have given rise to radiation protection. Utilizing radiation while reducing its risk as much as feasible is the goal of radiation protection [7,8].

The most crucial component of radiation protection is shielding. Placing radiation-absorbing substances between the radiation source and the protected system is the foundation of shielding. Owing to exposures for ionizing radiation in applications like nuclear power plants, medicine, space and accelerators, shielding materials have been of great interest [9]. Recently, many authors evaluated different materials such as alloys [10], ceramics [11], polymers [12], glasses [13] and rocks [14] as shielding materials. Polymers, glass, natural rocks, and minerals, are thought to be the best and most effective solutions for defending against gamma photons with different energies extending from low to high energy spectrum due to defects in manufacturing and relatively high cost of alloys [13]. Rocks and minerals that are found naturally are widely accessible, cheap, and homogeneous in composition. They can be applied directly as a material for shielding or in a variety of ways, such as bricks, coarse and fine particles in concrete mixes, and shaped rocks [14].

Different rocks from different parts of the world have been studied as potential materials for nuclear radiation shielding due to their generally high density and ability to attenuate radiation [15]. Some studies have focused on specific types of sedimentary rocks, such as sandstone [16], while others have looked at a range of different rock types [17]. A study on the radiation shielding properties of sedimentary rocks was performed by Al-Saleh and Al-Jarallah [18]. In this study sedimentary rocks (sandstone, limestone and shale) were chosen as they are the most abundant rocks in Saudi Arabia. Gamma ray spectroscopy was used to measure the attenuation coefficients of these rocks for gamma rays of energies ranged from 662 to

\*Corresponding author e-mail: [faissalkhalil5@yahoo.com](mailto:faissalkhalil5@yahoo.com) (Faisal A. Ali)

EJCHEM use only: Received date here; revised date here; accepted date here

DOI: 10.21608/ejchem.2024.329676.10658

©2025 National Information and Documentation Center (NIDOC)

1332 keV. The theoretical values derived from the XCOM computer code were compared to the experimental data. The measured attenuation coefficients values were found to agree well with the theoretical values. The results indicate that sedimentary rocks can be used as gamma radiation shielding materials. On the other hand, a theoretical analysis using Phy-X/PSD and XCOM software in energy ranges of 1.0 keV to 100 GeV, as well as experimental testing in the energy range of 662 to 1275 keV, was performed on different types of rocks which have been collected from different parts of Turkey [19]. The results indicated that the coefficients of attenuation declined with increment of energies. A radiation shielding performance of Najran granite was evaluated by Khan et al. [20]. Experimental tests were done on granite samples to see how well they could block radiation at energies ranged from 59.5 to 1332 keV. It was found that due to high values of atomic cross sections of granite, they have good shielding efficiencies for low energy gamma rays. Moreover, granite may be suggested as appropriate replacements for  $\gamma$ -rays shielding applications in storage and conveying natural occurrence of radiation materials (NORM) and nuclear reactors, because they also possess a significant shielding properties for  $\gamma$ -rays with high energy.

In the present investigation, three igneous (granitic rocks) samples taken from various locations in Egypt were evaluated for their chemical and mineralogical compositions, petrographic characteristics, physical and mechanical properties, and radiation shielding properties. This research has been performed to look at the shielding behavior of these investigated rocks and compared with two types of concretes (ordinary concrete (OC) and reactive powder concrete (RPC)) experimentally and theoretically for neutrons and  $\gamma$ -rays due to the abundance of these rocks in Egypt with different origins.

## 2. Experimental work

### 2.1 Raw materials

Three different categories of Egyptian granitic rocks samples collected from three different quarries in Aswan, Verdi from Abo Marwa, New Halaib (Granodiorite) from Barramiya, and red granite from Um Shaggier. The studied rocks locations are listed in Table 1 and Fig. 1. Moreover, two different concrete samples namely, ordinary concrete (OC) and reactive powder concrete (RPC) were prepared according to ASTM standard and used for comparison as reference materials. More information on the preparation steps of the concretes can be found in our previous work [21]. The chemical compositions were conducted using X-ray fluorescence (XRF).

Table 1: Locations of studied granitic rocks.

Sample code	Sample name	Origen	Location	
			Longitudes E.	Latitudes N.
G1	Verdi	Abo Marwa – Aswan	33° 23' 45"	23° 05' 18"
G2	New Halaib	Barramiya	33° 47' 23"	25° 05' 16"
G3	Red granite	Um Shaggier	31° 36' 46"	23° 15' 30"



Fig. 1: Location map of studied granitic rocks.

## 2.2 Petrographic Analysis

The petrographic studies were performed at Egyptian Mineral Resources Authority (Central Laboratories Sector). Thin sections have been prepared for each rock for microscopic investigation using Ortholux Leitz microscope. The petrographic studies were carried out according to ASTM – C1721.

## 2.3 Density

Archimedes' principle was used to calculate the density of the materials under investigation in accordance with ASTM B328-96 Standard.

## 2.4 Apparent porosity

The measurements of apparent porosity were done on 50 mm cubes which have been cut out of cubes of 100 mm. The samples were placed in desiccators for 5 hours after had been dried at 120 °C for 24 hours. Finally, all the samples were placed into a container containing deionized water and left there for 48 hours. According to Eq. (1) [22], the apparent porosity ( $\rho$ ) % was calculated:

$$\rho (\%) = \left( \frac{W_s - W_d}{W_s - W_w} \right) \times 100 \quad (1)$$

Where;  $W_d$ ,  $W_w$  and  $W_s$  are the dry sample weight, the sample weight in water at saturated conditions and the saturated sample weight in air, respectively.

## 2.5 Compressive strength

Compressive strength testing was done in accordance with ASTM C170. The specimens were cut into cubes of 100 mm in length. Slowly, the load was applied using a universal compression machine.

## 2.6 Abrasion test

Abrasion rate was investigated in the laboratories of Housing & Building National Research Center (HBRC). The studied samples had a cross-sectional area 1 x 1 cm<sup>2</sup>. By using a rotating abrasion testing machine with a rate of rotation is 600 r.p.m, applied pressure 20 N, sand as abrasive material (25-36 mesh) and time 15 minutes was determined the loss in weight. Losing thickness (abrasion) was determined according to [23]. By using the following formula:

$$\text{Losing thickness (abrasion)} = (W1 - W2) / (A \times \rho)$$

Where;  $W1$  = Weight of specimen before abrasion,  $W2$  = Weight of specimen after abrasion,  $\rho$  = Sample density,  $A$  = Cross sectional area of the specimen.

## 2.7 Neutrons attenuation measurements

<sup>241</sup>Am-Be neutron source possesses activity of 100 mCi was aligned with (BF<sub>3</sub>) neutron detector for measuring the transmitted fluxes of two ranges of neutron energies (The slow neutron & neutron with energy greater than 10 keV). Eq. (2) [24] was used for deducing these fluxes:

$$I = I_0 e^{-\Sigma x} \quad (2)$$

Where  $\Sigma$  (cm<sup>-1</sup>) stands for macroscopic cross section, determined from the exponential relation slope between ( $x$ ) and ( $I$ ) which represent the thickness of barrier and the transmitted neutron intensity, respectively.  $I_0$  signifies the original incident intensity neutron. In order to determine measurements of slow neutrons, the collimated beams were delayed using a cube with a length of 7 cm prepared from polyethylene and put in the front of the source. Similarly, neutrons of energy lower than (10 keV) have been cut off using bulk of (B<sub>4</sub>C). Fig 2 displays the diagram of our experimental setup. Moreover, Eq. (3) [25] was utilized to estimate the highest error values of the neutron's macroscopic cross-section.

$$\Delta \Sigma = \frac{1}{x} \sqrt{\left( \frac{\Delta I_0}{I_0} \right)^2 + \left( \frac{\Delta I}{I} \right)^2 + \left( \ln \frac{I_0}{I} \right)^2 \left( \frac{\Delta x}{x} \right)^2} \quad (3)$$

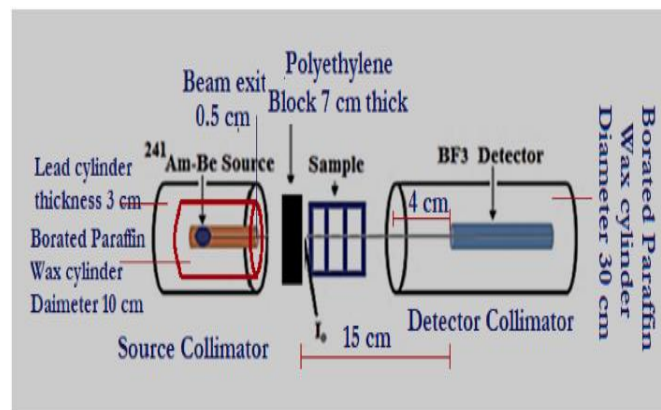


Fig. 2: Experimental setup for neutron detection

## 2.8 Measurements of $\gamma$ -rays attenuation and calculations

The  $\gamma$ -rays attenuation coefficients of investigated rocks as well as the reference concretes attenuation coefficients were determined using energy lines of (121.78, 344.27, 661.64, 778.9, 1112.4, 1173.23, 1332.51, and 1407.92 keV) which were released from (3.7  $\mu$ Ci Eu-152, 9.5  $\mu$ Ci Cs-137 and 4.9  $\mu$ Ci Co-60) radioactive sources. A diagram of our  $\gamma$ -ray spectrometer's experimental setup is revealed in Fig. 3.  $\gamma$ -rays transmitted beams through the examined materials were measured using 3" x 3" NaI(Tl) scintillation detector.

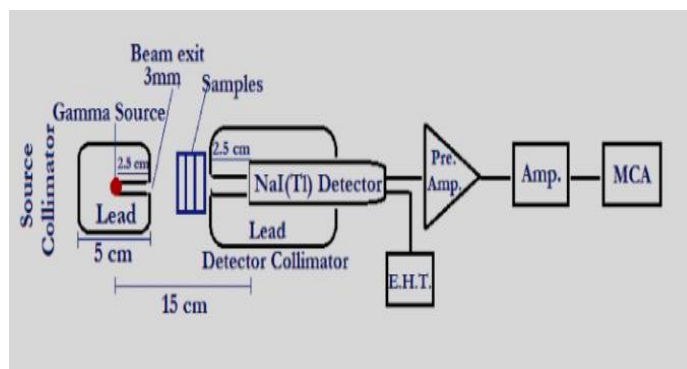


Fig. 3: Experimental setup for gamma ray detection.

The  $\gamma$ -ray transmission process through the investigated materials depends basically on the density of material and gamma ray energies.

The coefficients of linear attenuations of the investigated materials were calculated using Beer-Lambert's formula Eq. (4), while the mass attenuation coefficient was determined using Eq. (5) [25,26].

$$I = I_0 e^{-\mu x} \quad (4)$$

$$\sigma = \frac{\mu}{\rho} \text{ (cm}^2\text{/g)} \quad (5)$$

Additionally, the maximum error in the coefficient of mass attenuation has been determined using Eq. (6) [27].

$$\Delta\sigma = \frac{1}{x\rho} \sqrt{\left(\frac{\Delta I_0}{I_0}\right)^2 + \left(\frac{\Delta I}{I}\right)^2 + \left(\ln \frac{I_0}{I}\right)^2 \left(\frac{\Delta x\rho}{x\rho}\right)^2} \quad (6)$$

The sample's half value layer (HVL) was calculated using Eq. (7) [26].

$$\text{HVL} = \frac{\ln 2}{\mu} \text{ cm} \quad (7)$$

Where;  $\mu$  ( $\text{cm}^{-1}$ ),  $x$  and  $\sigma$  are the coefficient of linear attenuation, the thickness and the coefficient of mass attenuation, respectively.  $\sigma$  is independent of material density.

Depending on the mixture rule (Eq. 8), the calculated mass attenuation coefficient values for the sample compositions have been computed using WinXcom software (ver. 3.1) [25]. The Mean Free Path (MFP) was calculated using Eq. (9) [22].

$$\sigma_T = \sum_i^n W_i \left(\frac{\mu_i}{\rho_i}\right)_m \quad (8)$$

$$\text{MFP} = 1/\mu \text{ (cm)} \quad (9)$$

Where;  $\frac{\mu_i}{\rho_i}$  and  $W_i$  are the coefficient of mass attenuation for element in each mixture and the fractional weight for the elements into each mixture, respectively. The scan rate was 10 min for each reading.

## 3. Results and discussions

### 3.1 Petrographic Analysis

The thin sectional microscopic images for the samples under investigation are shown in Fig. 4. It is evident from Fig. 4-A that the G1 is mostly constituted of plagioclase feldspars (PL) (35-40%), quartz (QU) (25-30%), potash feldspars (P-FEL) (15-20%), biotite, and hornblende (BI) (10-12%) as essential minerals paired with rare opaque minerals (1%). Medium to fine grained quartz is found and anhedral to subhedral crystals of quartz intercalated with various mineral components are present. Plagioclase feldspars are found as medium- to coarse-grained prismatic crystals that range in shape from subhedral to anhedral. These crystals have a dusty, cloudy appearance with twin albitic lamellae. Some plagioclase crystals exhibit selective alteration in the core, which is corroded by perthite and quartz and somewhat sericitized. Small, pleochroic, chloritized, and muscovitized flakes of dark brownish biotite are present in nature. They primarily have iron oxide flecks and are connected to a few auxiliary minerals. Deep green pleochroic crystals of hornblende, which are closely related to biotite and quartz, perthite, and plagioclase, are found in nature.

On the other hand, G2, as seen in Fig. 4-B, takes into account old granites that are large and fine to medium grained. It is distinguished by joints and quartz veins. It mainly includes minerals such microcline (40-45), plagioclase (15-20), quartz (20-25), and biotite (12-15). Quartz has a euhedral structure and is colorless. Quartz, plagioclase, orthoclase, biotite, and iron oxides

make up the granite. The texture is equi-granular, and the grains range from coarse to medium in size. It occurs in a plutonic manner.

Additionally, Fig. 4-C demonstrates that G3, younger red granite, has traits with the renowned red granites of Aswan monumental, including morphologies, color, mineralogical compositions, and sizes of crystal. It has a subdual granular texture with coarse to very coarse-grained particles. The content from quartz crystals partially was deformed and micro-cracked in some parts. The Early Paleozoic and Late Proterozoic periods are signified by the younger red granites. These granites are widely dispersed, tiny, ovoid shallow level intrusions that signal the start of the stability of the Arabian-Nubian Shield's crust. G3 composite mainly from potash feldspars (50-55%), quartz (15-20%), plagioclase (15-20%), and mafic minerals (biotite and hornblende) (7-10%), with trace amounts of muscovite and opaque minerals. The main mineral composition of studied granite rocks was collected in Table 2.

**Table 2: Main mineral composition of granitic rocks.**

Mineral	G1	G2	G3
Quartz	25-30	20-25	15-20
Plagioclase feldspars	35-40	15-20	15-20
Potash feldspars	15-20	40-45	50-55
Biotite, and hornblende	10-12	12-15	7-10

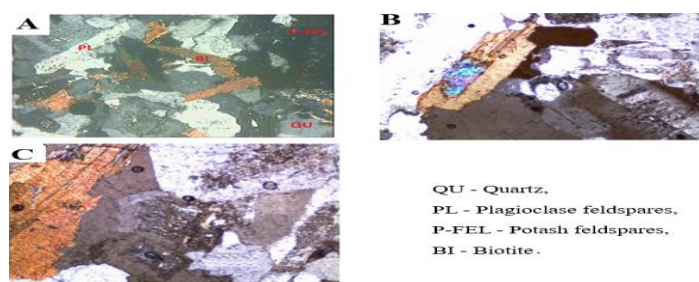


**Fig. 4: Microscopic image of granitic rocks samples.**

### 3.2 Chemical analysis

The chemical compositions of all investigated samples and reference concrete samples are displayed in Table 3. Clearly, the outcomes reveal that silicon oxide is the main major oxide while  $Al_2O_3$  is the second major oxide for granite samples with narrow ranges. All the investigated granites are characterized by enrichment in alkaline ( $Na_2O + K_2O$ ). This trend is due to the high contents of alkali feldspar. The relatively high content of  $MgO$  in G2 is attributed to the abundance of microcline and biotite compared with the other samples. The chemical analysis is in a good agreement with the mineralogical compositions. On the other hand, the chemical compositions of concrete samples show that  $SiO_2$  and  $CaO$  are the main major oxides. Further, the outcomes illustrate that RPC concrete contains higher  $Fe_2O_3$  compared with all the investigated samples.

**Table 3: Chemical analysis of granitic rocks, OC and RPC.**

Sample	G1	G2	G3	OC	RPC
$SiO_2$	75.60	69.93	71.52	45.110	60.890
$Fe_2O_3$	3.14	2.46	2.37	1.571	1.776
$CaO$	2.10	4.57	2.61	40.617	23.646
$MgO$	1.86	2.26	1.78	10.173	0.886
$Al_2O_3$	10.51	12.93	13.80	1.633	1.447
$TiO_2$	0.46	0.72	0.20	--	--
$MnO$	0.19	0.03	0.01	--	--
$Na_2O$	3.38	4.01	4.02	--	--
$K_2O$	2.67	2.98	3.31	--	--
$SO_3$	--	--	--	0.737	0.703
$C$	--	--	--	0.000	0.150
$Fe$	--	--	--	0.000	1.123
<b>L.O.I</b>	0.09	0.11	0.38	0.160	9.349

### 3.3 Physical and mechanical properties

The experimental values of the physical properties, density and porosity, for different rocks compared with OC and RPC are shown in Table 4. It is clear that the density of rocks is considered greater than that of the OC and RPC as reference materials. Further, their apparent porosities are lower than the reference concrete. These results encourage the authors to use these types of rocks as shielding materials for gamma rays. In addition to their chemical composition, which contain light elements made them favorable shielding materials for neutrons.

**Table 4: Physical and mechanical properties of granitic rocks, OC and RPC.**

Rock type	Properties			
	Bulk density (gm/cm <sup>3</sup> )	Apparent porosity (%)	Abrasion rate (mm)	Compressive strength (MPa)
<b>G1</b>	2.64	0.34	0.036	96.9
<b>G2</b>	2.56	0.47	0.062	89.54
<b>G3</b>	2.47	0.54	0.053	83.68
<b>OC</b>	2.39	9.54	0.121	30.43
<b>RPC</b>	2.44	1.67	0.047	110.89

The compressive strength ( $\sigma_c$ ) of the investigated rocks and reference concrete samples are given also in Table 4. It is obvious that, G1 gives the highest  $\sigma_c$  value (96.6 MPa) due to its fine-grained texture and it possesses high percentages of silica (75.60%) and iron oxides (3.14%) while G3 offers the lowest  $\sigma_c$  value (83.68 MPa), this behavior is attributed it has a coarse-to very coarse-grained texture. Furthermore, its content from quartz crystals partially were deformed and micro-cracked in some parts owing to the tectonic movements and environmental effects. Similarly, G2 gives  $\sigma_c$  value (89.54 MPa), owing to the grains are coarse to medium texture. Table 4 illustrates that, all granitic rocks give  $\sigma_c$  higher than OC (30.43 MPa), while the RPC exhibits  $\sigma_c$  (110.89 MPa) higher than the granitic rocks.

On the other hand, Table 4 reveals the abrasion rate of the investigated rocks compared with OC and RPC. Clearly, G1 gives the lowest value of abrasion rate (0.036 mm.) due to its high percentages of hard minerals contents such as quartz (25-30%) comparing with G2 and G3 as illustrated from Table 2. G2 and G3 give high abrasion rate (0.062, 0.053 mm.), respectively. This behavior is attributed to their high content of feldspar minerals (Plagioclase and Potash), which both consider about (65-75%) as shown in Table 2. Furthermore, all granitic rocks give abrasion rate lower than OC (0.121 mm.) due to its high porosity (9.54%), while the RPC exhibits abrasion rate (0.047 mm.) higher than G1 but lower than the others. This behavior may be attributed to its contents of fine powders.

### 3.4 Neutron

Borontrifluoride (BF<sub>3</sub>) tubes have been used to detect transmitted collimated beam of neutrons emitted from <sup>241</sup>Am-Be source with activity 100 mCi. Two ranges of neutrons (slow neutron & neutron with energy > 10 keV) were utilized for determining the neutron macroscopic cross-section ( $\Sigma$ ) of three granite types under investigation in addition to two types of concrete (RPC & O.C.) as a reference. Fig. 5 shows the ingredient in values of ( $\Sigma$ , cm<sup>-1</sup>) for all samples.

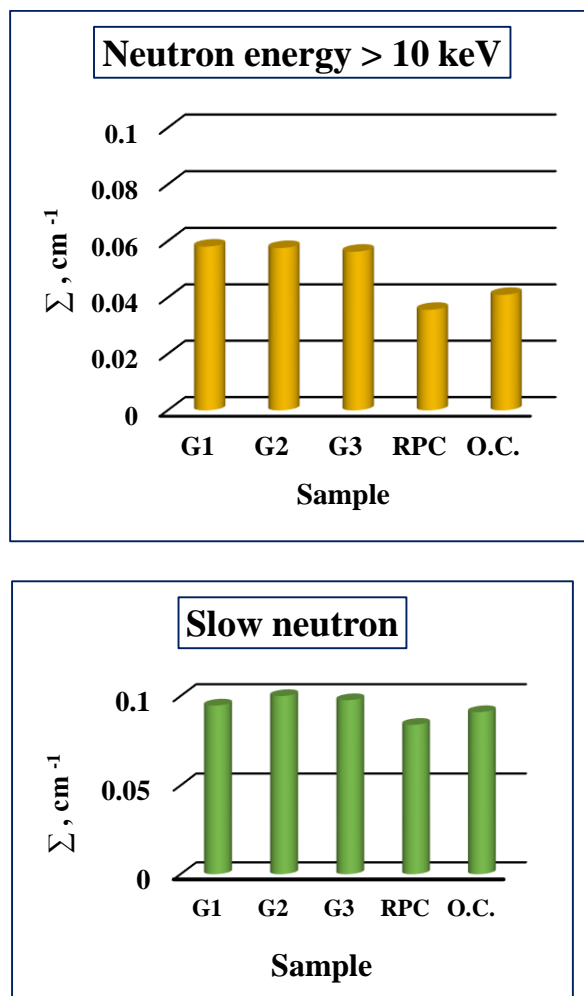


Fig. 5: Neutron energy type.

Table 5: Half value layer for granitic rocks, OC and RPC.

Energy (keV)	HVL (Cm)				
	G1	G2	G3	OC	RPC
121.78	2.34±0.16	2.51 ±0.20	2.04±0.18	3.26±0.26	2.60±0.16
344.27	3.43±0.18	3.63±0.30	3.19 ±0.18	3.33±0.29	3.64±0.09
661.64	3.47±0.03	3.30±0.04	3.32±0.02	4.17±0.21	4.09±0.02
778.9	3.18 ±0.32	4.82±0.70	4.02±0.61	5.63±0.55	4.36±0.21
964	5.35±0.48	4.77 ±0.30	4.46 ±0.37	5.59±0.61	4.93±0.59
1112.4	4.99±0.20	4.68±0.25	5.37±0.36	5.92±0.34	4.24±0.25
1173.23	4.79±0.09	4.38±0.14	4.67±0.12	5.17±0.16	4.51±0.09
1332.51	4.24 ±0.07	4.42 ±0.09	4.34 ±0.08	5.50±0.12	4.70±0.05
1407.24	5.09 ±0.27	4.96 ±0.24	4.80 ±0.33	6.41±0.56	4.82±0.19

The results indicate that the slow neutron macroscopic cross-section values for samples are nearly twice their values in case of neutron with energy  $> 10$  keV macroscopic cross-section  $\Sigma_{10}$  which may be attributed to the interactions between more abundant Si-28 nuclei in chemical composition of three granite types and the slow neutron. Whereas its value in the neutron energy less than 10 keV, the scattering of neutrons by Si-28 is dominated [24]. Moreover, the results demonstrate that the values of  $\Sigma_s$  and  $\Sigma_{10}$  of three types of rocks are greater than that of OC and RPC concretes. Which may be owing to the elastic scattering interaction of neutrons with light nuclei as oxygen, silicon, and Al in rocks is much more than in case of OC and RPC concretes. Also there is a more porosity in OC and RPC than that of rocks. Mean free path MFP is the other important nuclear parameter which used to compare the preference of different types of samples to be used as shields from neutrons with different energies. Fig. 6 shows the behavior of MFP values of three rocks, OC and RPC concretes which illustrates that the MFP of slow neutron is more effective than that of neutron with energy  $> 10$  keV in all investigated samples. On the other hand, it is clear that the value of MFP for rocks types is more effective than that of OC and RPC. This behavior may be due to the light nuclei of oxygen, silicon, and Al in rocks.

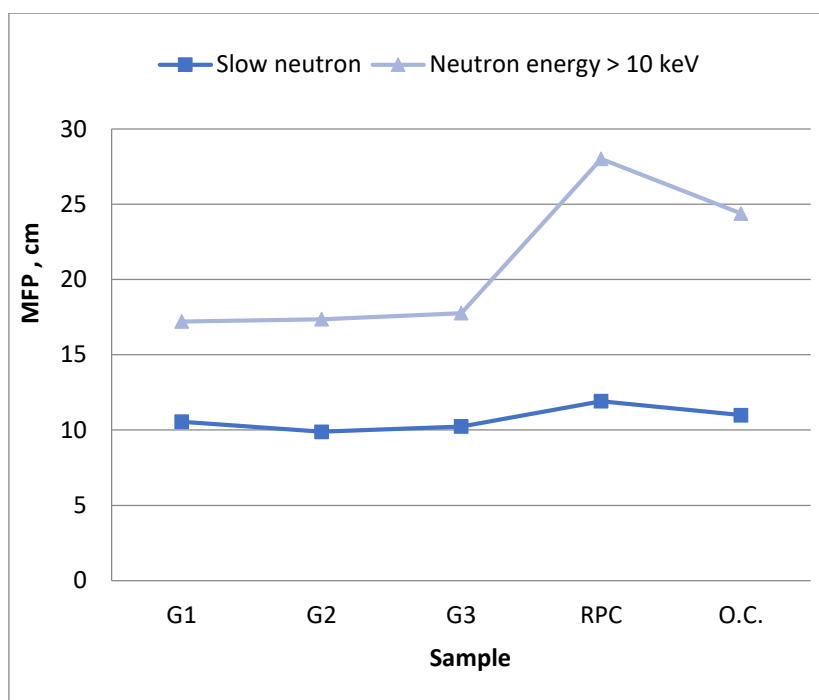


Fig. 6: Mean free path MFP of the investigated granitic rocks, OC and RPC.

### 3.5 Gamma-rays

The experimental and calculated coefficient of attenuation values for three granite types, OC and RPC are presented in Fig. 7.

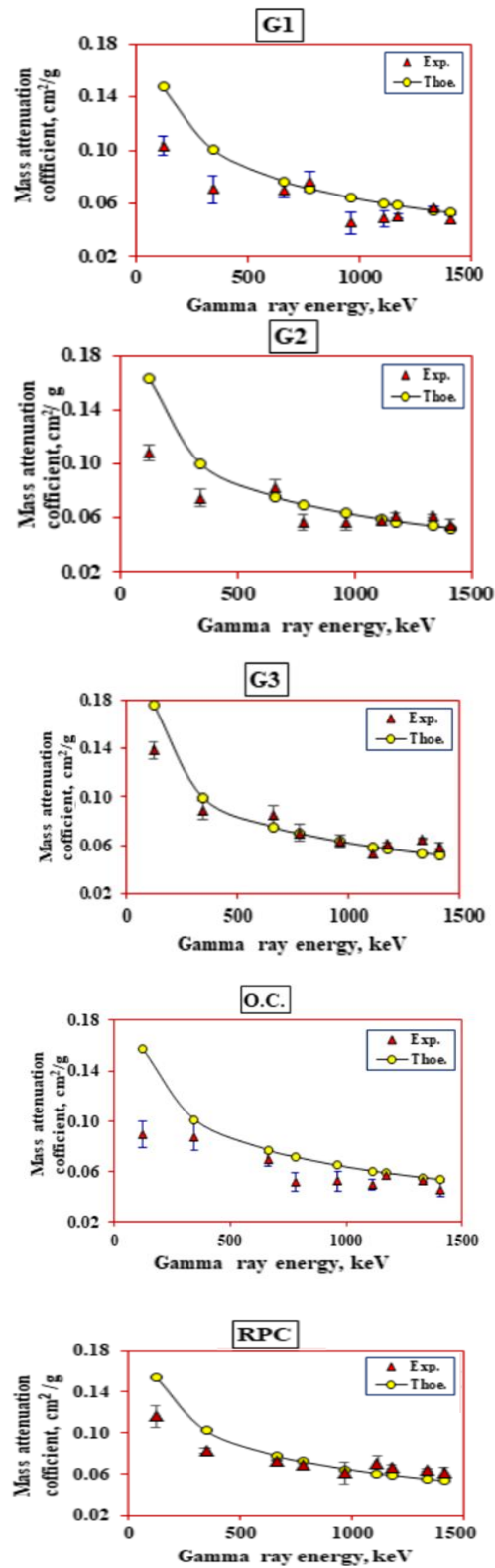


Fig. 7: Mass attenuation coefficient of granitic rocks, OC and RPC.

The  $\gamma$ -rays coefficients of attenuation for samples under consideration were deduced using  $\gamma$ -rays with energies ranging from 121 keV to 1400 keV. The intensities value of  $\gamma$ -rays transmitted through sample barriers have been given as a function of barrier thicknesses. The values of total mass attenuation coefficients ( $\sigma$ ) for samples have been extracted from the attenuation curves slopes. Clearly, the findings illustrate a good agreement between experimental values and the value which were calculated using WinXcom program.

Although the used  $\gamma$ -rays energies were up to 1400 keV, this wide range can be divided into two distinct zones [25,26]: (i) energies range from 121 keV to 344 keV. In this zone, there is a sharp decrease in the values of mass attenuation coefficient as a  $\gamma$ -ray energy increase which can be attributed to the prominent reaction between the gamma-ray and investigated samples is a photoelectric effect. (ii) Energies range from 344 keV up to 1400 keV, this zone characterizes with a slight decrease in  $\sigma$  values with increasing  $\gamma$ -ray energies. The behavior could be attributed to the Compton scattering process [27]. On the other hand, it is clear from Fig. 8 that, almost all used gamma rays energies, granite samples have attenuation ability more than OC and less than RPC that can be explained as RPC was reinforced by steel fibers, which considered favorable shield materials for gamma-rays, and has low porosity than that of OC [24]. Table 5 shows the values of half value layer HVL as a function of  $\gamma$ -rays energies which illustrate that the three granite types have attenuation behavior favorable than that of OC and RPC in all used  $\gamma$ -rays energies which could be attributed to the hardness of granite as discussed before.

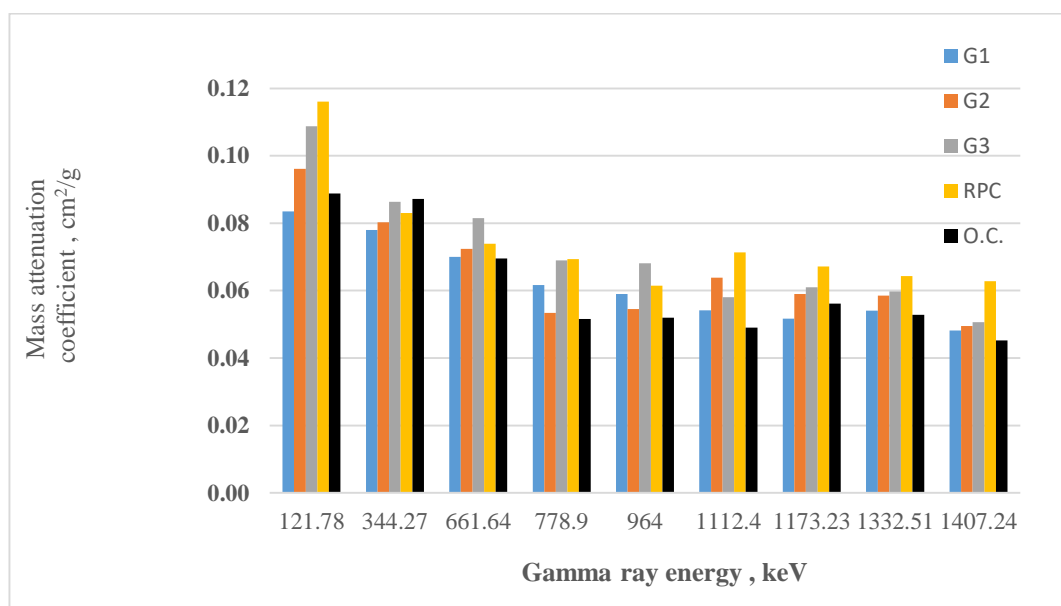


Fig. 8: Mass attenuation coefficient for all samples at different gamma energy

#### 4. Conclusions

The mineralogical compositions, petrographic characteristics, physical and mechanical properties, as well as the radiation shielding characteristics of some Egyptian granitic rocks were investigated and compared with two types of concrete as reference materials. The outcomes illustrated that, the granitic rocks are better shielding materials for both fast and low neutrons. In the case of fast neutrons, the  $\Sigma_{10}$  for rocks is greater than that of OC and RPC with about 45%, while in the case of slow neutrons,  $\Sigma_S$  is greater than that of OC and RPC with about 18%. The granitic rock samples have attenuation ability gamma-rays more than OC and less than RPC. Therefore, granitic rocks can be used as structure materials for nuclear diagnostic centers and medical diagnostic radiology facilities owing to their radiation shielding properties and low cost. The calculated mass attenuation coefficient values and the experimental values showed excellent agreement.

#### 5. Funding

The study did not receive funding.

#### 6. Declarations

Conflict of Interest Statement: The authors confirm that there are no conflicts of interest between themselves, any individuals, or authorities involved in the study, and they solely own the research idea and its findings. Consequently, the authors

declare the following; the article is original, written by the specified authors who are fully aware of its content and consent to its submission, it has not been previously published, it is not being considered for publication elsewhere, and no conflict of interest exists.

## 7. Acknowledgement

Thanks to editors and anonymous reviews for their help and constructive comments.

## 8. Reference

- [1] S.H. Shin, W.N. Choi, S. Yoon, U.J. Lee, H.M. Park, S.H. Park, Y.J. Kim, H.R. Kim, Radiological analysis of transport and storage container for very low-level liquid radioactive waste, *Nucl. Eng. Technol.* 53 (2021) 4137–4141. <https://doi.org/10.1016/j.net.2021.06.024>.
- [2] J.N. Eiras, C. Payan, S. Rakotonarivo, V. Garnier, Experimental modal analysis and finite element model updating for structural health monitoring of reinforced concrete radioactive waste packages, *Constr. Build. Mater.* 180 (2018) 531–543. <https://doi.org/10.1016/j.conbuildmat.2018.06.004>.
- [3] F. Gera, The classification of radioactive wastes, *Health Phys.* 27 (1974) 113–121. <https://doi.org/10.1097/00004032-197407000-00015>.
- [4] M.U. Khandaker, D.A. Bradley, H. Osman, M.I. Sayyed, A. Sulieman, M.R.I. Faruque, K.A. Naseer, A.M. Idris, The significance of nuclear data in the production of radionuclides for theranostic/therapeutic applications, *Radiat. Phys. Chem.* 200 (2022). 110342. <https://doi.org/10.1016/j.radphyschem.2022.110342>.
- [5] M.I. Sayyed, M.K. Hamad, M.H.A. Mhareb, K.A. Naseer, K.A. Mahmoud, M.U. Khandaker, H. Osman, B.H. Elesawy, Impact of modifier oxides on mechanical and radiation shielding properties of B<sub>2</sub>O<sub>3</sub>-SrO-TeO<sub>2</sub>-RO glasses (Where RO = TiO<sub>2</sub>, ZnO, BaO, and PbO), *Appl. Sci.* 11 (2021). <https://doi.org/10.3390/app112210904>.
- [6] Rossi, Harald H., and Charles W. Mays. "Leukemia risk from neutrons." *Health Physics* 34.4 (1978): 353-360.
- [7] A. Ottolenghi, V. Smyth, K.R. Trott, Assessment of cancer risk from neutron exposure - The ANDANTE project, *Radiat. Meas.* 57 (2013) 68–73. <https://doi.org/10.1016/j.radmeas.2012.10.017>.
- [8] A. Saeed, S. Alomairy, C. Sriwunkum, M.S. Al-Buriahi, Neutron and charged particle attenuation properties of volcanic rocks, *Radiat. Phys. Chem.* 184 (2021) 109454. <https://doi.org/10.1016/j.radphyschem.2021.109454>.
- [9] M.S. Al-Buriahi, C. Sriwunkum, H. Arslan, B.T. Tonguc, M.A. Bourham, Investigation of barium borate glasses for radiation shielding applications, *Appl. Phys. A Mater. Sci. Process.* 126 (2020). <https://doi.org/10.1007/s00339-019-3254-9>.
- [10] A. Saleh, R.M. Shalaby, N.A. Abdelhakim, Comprehensive study on structure, mechanical and nuclear shielding properties of lead free Sn–Zn–Bi alloys as a powerful radiation and neutron shielding material, *Radiat. Phys. Chem.* 195 (2022) 110065. <https://doi.org/10.1016/j.radphyschem.2022.110065>.
- [11] E. Hannachi, Y. Slimani, M.I. Sayyed, K.A. Mahmoud, Synthesis of lead oxide doped SmBa<sub>2</sub>Cu<sub>3</sub>O<sub>y</sub> ceramic systems as efficient shields against  $\gamma$  radiations: Structure, radiation attenuating capacities, and optical features, *Ceram. Int.* 48 (2022) 31902–31908. <https://doi.org/10.1016/j.ceramint.2022.07.124>.
- [12] M.R. Kaçal, F. Akman, M.I. Sayyed, Evaluation of gamma-ray and neutron attenuation properties of some polymers, *Nucl. Eng. Technol.* 51 (2019) 818–824. <https://doi.org/10.1016/j.net.2018.11.011>.
- [13] Al-Buriahi, Mohammed Sultan, et al. Investigation of barium borate glasses for radiation shielding applications. *Applied Physics A* 126.1 (2020): 68.
- [14] M.S. Al-Buriahi, V.P. Singh, Comparison of shielding properties of various marble concretes using GEANT4 simulation and experimental data, *J. Aust. Ceram. Soc.* 56 (2020) 1127–1133. <https://doi.org/10.1007/s41779-020-00457-1>.
- [15] S.S. Obaid, M.I. Sayyed, D.K. Gaikwad, P.P. Pawar, Attenuation coefficients and exposure buildup factor of some rocks for gamma ray shielding applications, *Radiat. Phys. Chem.* 148 (2018) 86–94. <https://doi.org/10.1016/j.radphyschem.2018.02.026>.
- [16] A. Mansour, M.I. Sayyed, K.A. Mahmoud, E. Şakar, E.G. Kovaleva, Modified halloysite minerals for radiation shielding purposes, *J. Radiat. Res. Appl. Sci.* 13 (2020) 94–101. <https://doi.org/10.1080/16878507.2019.1699680>.
- [17] B. Oto, N. Yildiz, F. Akdemir, E. Kavaz, Investigation of gamma radiation shielding properties of various ores, *Prog. Nucl. Energy.* 85 (2015) 391–403. <https://doi.org/10.1016/j.pnucene.2015.07.016>.
- [18] K.A. Mahmoud, M.I. Sayyed, O.L. Tashlykov, Gamma ray shielding characteristics and exposure buildup factor for some natural rocks using MCNP-5 code, *Nucl. Eng. Technol.* 51 (2019) 1835–1841. <https://doi.org/10.1016/j.net.2019.05.013>.
- [19] A. Khan, A. Al alhareth, S. Mobark, W. Al-Mahri, N. Al- Sharyah, S. Al- Zmanan, H.B. Albargi, A.M. Abdalla,

- Experimental and theoretical investigations of the  $\gamma$ -rays shielding performance of rock samples from Najran region, *Ann. Nucl. Energy.* 183 (2023) 109676. <https://doi.org/10.1016/j.anucene.2022.109676>.
- [20] V.P. Singh, N.M. Badiger, N. Kucuk, Determination of Effective Atomic Numbers Using Different Methods for Some Low- Z Materials , *J. Nucl. Chem.* 2014 (2014) 1–7. <https://doi.org/10.1155/2014/725629>.
- [21] M.M. Sadawy, M.T. Nooman, Influence of nano-blast furnace slag on microstructure, mechanical and corrosion characteristics of concrete, *Mater. Chem. Phys.* 251 (2020) 123092. <https://doi.org/10.1016/j.matchemphys.2020.123092>.
- [22] M.M. Arfa, M.M. Sadawy, M.T. Nooman, A.T.M. Farag, R.M. El Shazly, The influence of heating on mechanical and nuclear properties of reactive powder concrete as a protective shield in nuclear facilities, *Prog. Nucl. Energy.* 143 (2022) 104046. <https://doi.org/10.1016/j.pnucene.2021.104046>.
- [23] Reda Selim, “Exploitation Management of Ornamental stone (Firan-Solaf region, South Sinai)”. Egypt, Msc. thesis PP. 62, 2006 .
- [24] M.M. Sadawy, R.M. El Shazly, Nuclear radiation shielding effectiveness and corrosion behavior of some steel alloys for nuclear reactor systems, *Def. Technol.* 15 (2019) 621–628. <https://doi.org/10.1016/j.dt.2019.04.001>.
- [25] S. Singh, A. Kumar, K.S. Thind, G.S. Mudahar, Measurements of linear attenuation coefficients of irregular shaped samples by two media method, *Nucl. Instruments Methods Phys. Res. Sect. B Beam Interact. with Mater. Atoms.* 266 (2008) 1116–1121. <https://doi.org/10.1016/j.nimb.2008.02.019>.
- [26] C.W. Hong, J. Il Lee, J.H. Ryu, Effect of copper slag as a fine aggregate on the properties of concrete, *J. Ceram. Process. Res.* 18 (2017) 324–328.
- [27] H.S. Alorfi, M.A. Hussein, S.A. Tijani, The use of rocks in lieu of bricks and concrete as radiation shielding barriers at low gamma and nuclear medicine energies, *Constr. Build. Mater.* 251 (2020) 118908. <https://doi.org/10.1016/j.conbuildmat.2020.118908>.